*Article*

# Incremental Dynamic Analysis Considering Main Aftershock of Structures Based on the Correlation of Maximum and Residual Inter-Story Drift Ratios

**Jiting Qu * and Chuyun Pan**

School of Civil Engineering, Faculty of Infrastructure Engineering, Dalian University of Technology, Dalian 116024, China; pcy@mail.dlut.edu.cn
* Correspondence: qjt@dlut.edu.cn

**Abstract:** Aftershocks often occur after strong earthquakes and aggravate structural damage. Commonly, the incremental dynamic analysis (IDA) considering the main aftershocks only used a single index such as the maximum or the residual inter-story drift ratio. However, results of IDA using different indices may suggest that a structure has collapsed but is still repairable, which is not realistic. Given these shortcomings, this paper proposes selecting two indices in the IDA method based on the correlation between the maximum and the residual inter-story drift ratio, considering the main aftershocks. The influence of the double-indices model on the structural vulnerability analysis was discussed by establishing a commercial building in SAP2000 software, and single-index and double-index IDA were carried out, respectively. The joint distribution probability of the two indices under fixed seismic intensity was also calculated. The difference between the single-index and double-index IDA results was compared considering both the main shock and the main aftershock. The results showed that the effect of aftershocks would improve the correlation coefficient between the maximum and the residual inter-story drift ratio, and the building model has a higher probability of overrun after considering the correlation of the two indices. This paper provides a new method for IDA and vulnerability analysis using multiple indices.

**Keywords:** inter-story drift ratio; IDA method; joint index; vulnerability analysis

## 1. Introduction

Historical data show that aftershocks often occur after an earthquake [1], and prominent examples include the Tangshan Earthquake in 1976 [2], the Northridge Earthquake in 1994 [3], the Wenchuan Earthquake in 2008 [4], the Tohoku Earthquake [5] in 2011, and the Christchurch Earthquake in 2011 [6]. Among them, the Tohoku earthquake caused a direct economic loss of 200 billion dollars [7]. After the Christchurch earthquake, more than 100,000 houses were damaged, and 10,000 houses needed to be demolished. The total cost of reconstruction estimated by the New Zealand government reached 40 billion dollars [8]. For buildings, when structural members undergo the plastic deformation stage under the action of the main shock and later experience the effect of aftershocks again, the damage accumulates, and the possibility of building collapse increases significantly. Therefore, in the study of the seismic performance of structures, it is of great practical significance to consider the collapse performance of a structure under the effect of aftershocks. In order to explore the influence of main aftershocks on seismic performance and seismic resilience of different types of structures, incremental dynamic analysis (IDA), vulnerability analysis, response surface method, Monte Carlo simulations, random vibration approaches, and adaptive support vector regression models are used [9–12]. The methods of IDA and vulnerability analysis are used in this paper.

The IDA was first proposed by Bertero [13] in 1977, and it is based on the dynamic elasto-plastic time history analysis. Later, and after a research study by Vamvatsikos et al. [14], the

method has been widely used in seismic capacity analysis and overall collapse performance evaluation of frames. In recent years, scholars have carried out various research on IDA. In terms of improving computational efficiency, a simplified modal incremental dynamic analysis (MIDA) method based on modal pushover analysis (MPA) [15,16], a simplified IDA method based on equivalent dual degree of freedom (EDDOF) [17], a simplified IDA method based on fast nonlinear analysis (FNA) [18] and an IDA method based on force analogy method (FAM) [19] were proposed. In terms of evaluation and application of IDA, Zhou et al. [20] applied the IDA method to the performance evaluation of high-rise hybrid structures, and considered that it is reasonable to use the inter-story drift ratios as the response parameter. Wu et al. [21] used the IDA method to evaluate the seismic performance of a steel frame structure, and found that the IDA curve obtained by Sa as the IM parameter had better convergence. Charney [22] demonstrated the advantages of using IDA in the sensitivity analysis of structures to a variety of parameters. As far as research objects are concerned, IDA has been widely used to analyze various structures such as buildings, stations, docks, and railways [23–25].

In the IDA under the action of main aftershocks, structural deformation, structural energy consumption, and local structural damage are generally used as a basis for evaluation. Generally, one of the above indices is used to evaluate and judge the seismic performance of a structure. The maximum inter-story drift ratio can accurately reflect the damage degree and the performance stage of the structure, which is directly related to the collapse resistance of the structure and the damage degree of the component [26]. The Park-Ang damage index takes into account the energy dissipation capacity of the structure, which can reflect the cumulative damage of buildings under aftershocks, and is mostly used in concrete structures. The maximum compressive strain is an important criterion for judging the local damage of structures. Liel et al. [27] proposed median column drift ratio (CDR) as the criterion for judging whether the column in the structure can have shear failure and vertical bearing capacity loss, and ultimate roof drift ratio ($RDR_{ult}$) as the basis for measuring structural ductility. Collapse margin ratio is selected as the normalization parameter because it is the basis for the code-defined maximum considered earthquake at most sites [28]. Critical demand-to-capacity ratio can take the uncertainty induced by the ground motion as well as the uncertainty associated with the definition of capacity into consideration [29]. In order to explore the overall deformation and collapse resistance of the structure under the action of main aftershocks, previous research studies considered the maximum inter-story drift ratio as the main index to define the limit state of the structure [30–33], and analyzed the vulnerability of wooden structures, concrete structures, and steel frame structures with masonry filling under main aftershocks. Marina et al. [34] considered the roof drift of the structure as the structural response index, and used three different statistical methods (IDA method, maximum likelihood fit for truncated IDA, and maximum likelihood estimation (MLE) method) to process IDA data, completed the vulnerability analysis under the action of main shock and main aftershock, and compared the difference in structural response. In addition, Yang et al. [35] considered the Park-Ang damage index as the structural response parameter to study the impact of aftershocks on the damage accumulation of frame step-terrace structures. Zhao et al. [36] considered the maximum compressive strain of concrete as the measuring standard, and the incremental dynamic analysis of the reinforced concrete nuclear island plant under the aftershock was carried out to discuss the impact of aftershock on the vulnerability of the plant.

Several scholars considered two indices to analyze the structures based on the IDA method. Baikuntha and Osman [37] selected the maximum inter-story drift ratio as the index to carry out the IDA for the main and aftershocks of the moment-resisting frame, before and after the addition of the super elastic viscous damper. In order to explore the recovery performance of the two types of structures, the residual inter-story drift ratio was selected as the index to carry out the IDA of the frame damaged by the aftershock. Xu et al. [38] selected the maximum inter-story drift ratio and Park-Ang damage index to analyze the vulnerability of a concrete frame structure under main aftershock based on the

IDA method. The authors found that the probability of reaching the same performance level of the structure is different when the two indices are selected to analyze the structure. Shi et al. [39] selected the residual inter-story drift ratio and the maximum inter-story drift ratio as the structural response indices. Based on the IDA, the vulnerability analysis of the moment-resisting frame before and after the addition of the shape memory alloy frame, under the action of the main aftershock, was carried out. Among them, the excess value of the residual inter-story drift ratio was directly calculated by the maximum transient story drift and story drift at yield.

In the IDA quantile calculation results, although the median of the ground motion intensity corresponding to the residual inter-story drift ratio and the maximum inter-story drift ratio was not much different, the traditional vulnerability analysis method cannot be used to calculate the subsequent excess probability without assuming the correlation between the two sets of data. In conclusion, existing studies on IDA using two indices mainly focused on the impact of aftershocks on the structure or the change of structural performance corresponding to different indices after the change of building system, and did not analyze the correlation of the two indices.

Therefore, based on the limitations of previous research studies, a double-index IDA method is presented considering the correlation between two indices. The maximum inter-story drift ratio and the residual inter-story drift ratio are selected as two indices, which can measure the seismic performance and the repairability of structures, respectively. In the definition of structure overrun, the scope of the two indices should be considered simultaneously, which can solve the problem that the probability of structural overrun is not unique under the condition of definite ground motion intensity. IDA data were obtained by using the cubic Bezier interpolation function, which makes data processing easier and curve smooth. Numerical analyses are illustrated to verify effectiveness and feasibility of the new method, which supplies beneficial reference to IDA and vulnerability analysis.

## 2. Incremental Dynamic Analysis Method Based on Double-Index

The IDA method amplifies the same seismic wave in a certain proportion and inputs the ground motion into the building structure step by step. By obtaining the maximum response curve of the structure under different amplifying proportion coefficients of seismic wave, the IDA curve is drawn. Considering the diversity of ground motions, multiple ground motions are generally used for IDA of structures to reduce the discreteness and draw IDA curve clusters. The selection of ground motion Intensity Measure (IM) and structural Damage Measure (DM) is an important part of the IDA. The IM mostly selects peak ground acceleration (PGA), peak ground velocity (PGV), and elastic acceleration response spectrum $S_a(T_1, 5\%)$. Recently, extensive work has been carried out to propose more suitable IMs for different structures, such as vector-valued IMs and advanced scalar IMs [40,41], which represent broader period ranges of structures [42–44]. The DM, also called the structural performance parameter, usually selects maximum inter-story drift ratio, node rotation, and maximum base shear. According to different structures and research fields, different and multiple indices can be selected. For specific selection methods, please refer to Vamvatsikos and Cornell [14].

The double-index IDA method requires two DMs to be selected based on one IM. The selected ground motion records are with the amplitude modulation, which are input into the established structural model in the form of time–history curves, and the nonlinear dynamic analysis is performed. Under the same IM, two DM values are extracted (in this paper, the maximum inter-story drift ratio and residual inter-story drift ratio were selected), and a number of data points were marked on the coordinate axis with DM as the abscissa and IM as the ordinate. The logarithmic data points were simulated by the cubic Bezier interpolation function, and IDA curve clusters of two types of DMs were drawn. Under the same IM, the two DMs are assumed to be lognormal in two dimensions. The specific steps are shown in Figure 1. After selecting two DMs, IDA was performed for the two DMs and

two IDA curve clusters were obtained. Then, the DMs of the two structures under the same ground motion intensity were extracted, and the correlation between the two sets of data was considered for analysis. Two DM values can be output simultaneously under the same amplitude modulation coefficient, so the computational efficiency of the double-index IDA method is not affected.
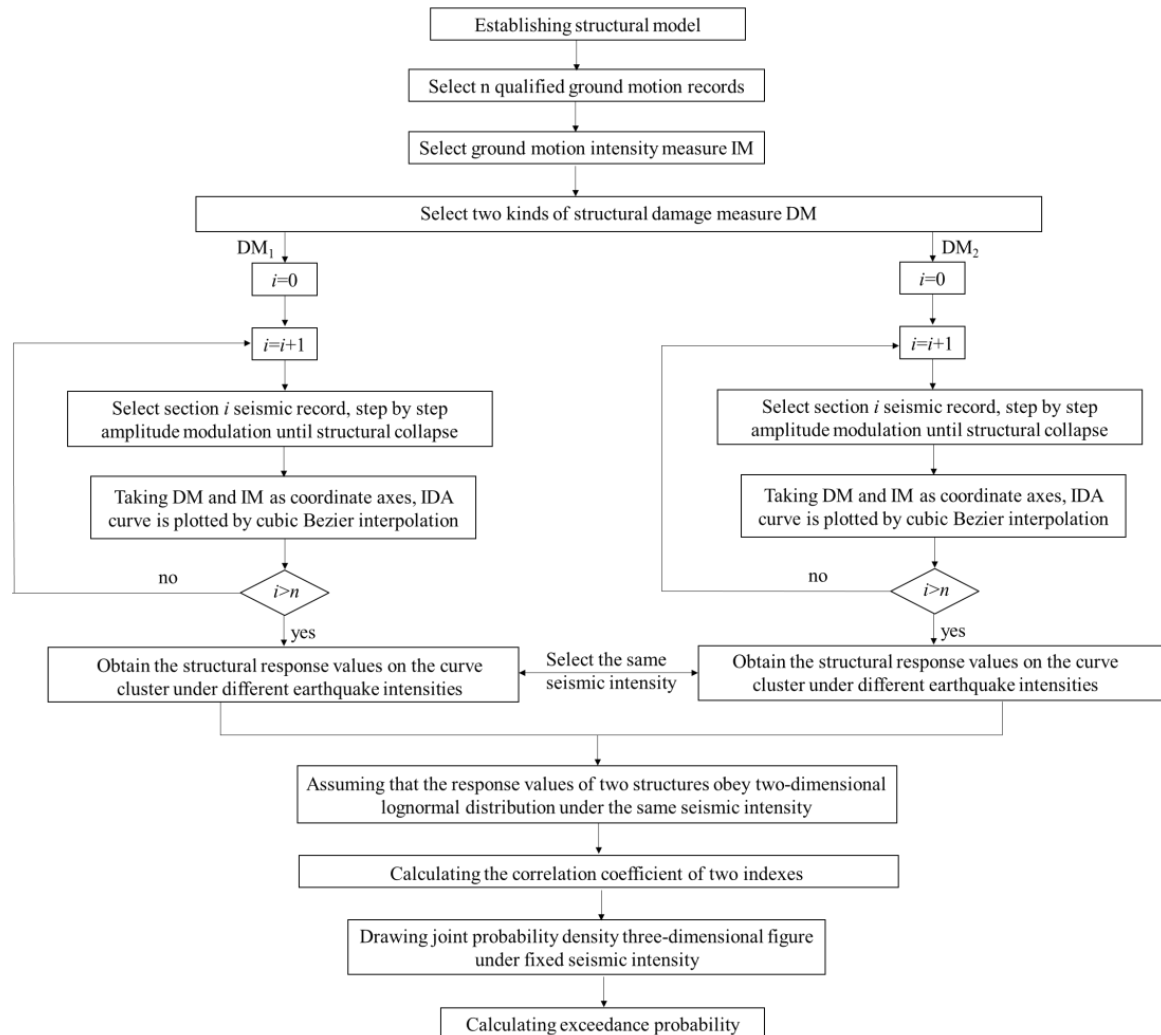


**Figure 1.** Steps of IDA method based on double index.

In order to obtain a smooth IDA curve, the cubic Bezier interpolation function is used to simulate the data points composed of IM and DM, and the approximate formula is used to obtain the function values at different points on the curve. The approximate formula of the cubic Bessel interpolation is as follows [45]:

$$F(t) = (1-t)^3 P_1 + 3t(1-t)^2 P_2 + 3t^2(1-t)P_3 + t^3 P_4, \qquad (1)$$

where $F(t)$ is the expression of the curve between every two points, and the value range of $t$ is [0, 1]. $P_1$, $P_2$, $P_3$, and $P_4$ are the four control points of the curve.

When drawing the quantile value curve, the DM statistics method is adopted. According to the principle of statistics, it is assumed that IM presents a lognormal distribution of the conditional probability when DM = $x$, which can be expressed as follows:

$$\ln(\mathrm{IM}|\mathrm{DM} = x) \sim \mathrm{N}\left(\mu, \sigma^2\right), \qquad (2)$$

where $x$ represents a number that a DM can get, $\mu = \ln_{\eta IM|DM=x}$ is the mean value of the normal distribution, and $\sigma = \beta_{IM|DM=x}$ is the standard deviation of the normal distribution.

By normalizing the normal distribution and making $Z \sim N(0, 1)$, the previous equation became as follows:

$$\frac{\ln(IM|DM = x) - \mu}{\sigma} = \frac{\ln(IM|DM = x) - \ln \eta_{IM|DM=x}}{\beta_{IM|DM=x}} \sim N(0, 1). \tag{3}$$

According to the properties of the standard normal distribution, $\Phi(1) = 0.84$, $\Phi(0) = 0.5$, and $\Phi(-1) = 0.16$. $\Phi$ is the cumulative distribution function of the standard normal distribution. It can be obtained as follows:

$$\Phi(0) = P\left[\frac{\ln IM - \ln \eta_{IM|DM=x}}{\beta_{IM|DM=x}} \leq 0\right] = P\left[IM \leq \eta_{IM|DM=x}\right] = 50\%, \tag{4}$$

$$\Phi(1) = P\left[\frac{\ln IM - \ln \eta_{IM|DM=x}}{\beta_{IM|DM=x}} \leq 1\right] = P\left[IM \leq \eta_{IM|DM=x} \cdot e^{\beta_{IM|DM=x}}\right] = 84\%, \tag{5}$$

$$\Phi(-1) = P\left[\frac{\ln IM - \ln \eta_{IM|DM=x}}{\beta_{IM|DM=x}} \leq -1\right] = P\left[IM \leq \eta_{IM|DM=x} \cdot e^{-\beta_{IM|DM=x}}\right] = 16\%. \tag{6}$$

Therefore, it is necessary to obtain the corresponding IM values of each IDA curve when DM = $x$. When drawing IDA curve clusters, the Bessel interpolation formula can be used to obtain the approximate function expression between every two data points. To obtain the $Y$-axis coordinates corresponding to a point on the curve, independent variables need to be substituted into the piecewise function. This method is convenient for data processing.

It is necessary to judge the structural damage not only from the perspective of security, but also to consider the local failure and post-earthquake restoration performance of a building. Different analysis directions need to choose different indexes. The two-index IDA of this paper is to choose two different indexes, and the repairability of the structure can be considered on the basis of structural safety. More accurate results can be obtained compared with single-index IDA.

## 3. Numerical Analysis

### 3.1. Basic Structure Information

This paper considers a six-story steel structure commercial building as an example [46]. The first and second floors of the building are parking lots, the third to fifth floors include commercial shops, and the sixth floor includes catering shops. The height of each layer is 4.50 m, and the typical layout of the building structure is shown in Figure 2. All the steel of the steel frame structure is Q345 strength grade, that is, the yield strength of steel is 345 Mpa. Section dimensions of components are shown in Table 1.
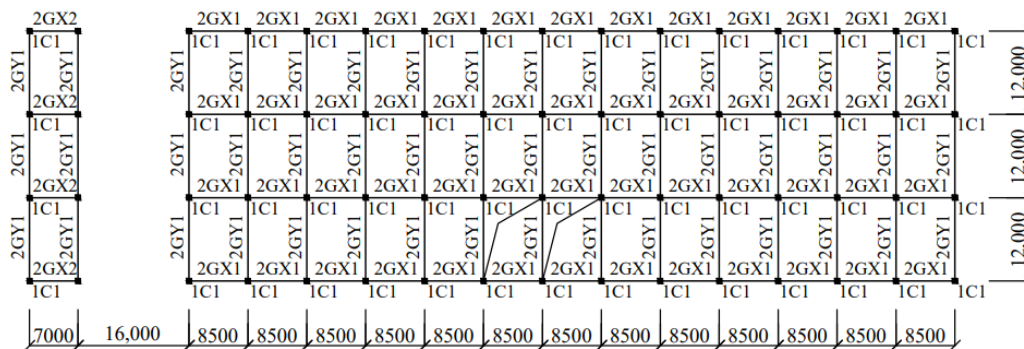


**Figure 2.** Typical layout of the building structure.

**Table 1.** Component section attributes.

| Component Type | Floor | Member Number | Section Properties |
|---|---|---|---|
| Beam | Roof | GX1 | HN700 × 250 × 12 × 22 |
| | | GY1 | HN700 × 350 × 14 × 28 |
| | 6 | GX1 | HN800 × 300 × 14 × 22 |
| | | GY1 | HN800 × 400 × 16 × 22 |
| | 5 | GX1 | HN800 × 300 × 14 × 28 |
| | | GY1 | HN800 × 400 × 16 × 32 |
| | 4~1 | GX1 | HN900 × 300 × 16 × 28 |
| | | GY1 | HN900 × 400 × 16 × 28 |
| Column | 6~4 | C1 | 700 × 700 × 25 |
| | 3~1 | C1 | 700 × 700 × 28 |

SAP2000 software was used to establish the structural model. It can complete the creation and modification of the model, the analysis and execution of the calculation results, the inspection and optimization of the structural design, and the graphic display of the calculation results (including displacement curve, response spectrum curve, acceleration curve of time history response); it can calculate and analyze the simplest problems to the most complex engineering projects. Nonlinear layered shells are selected for the plate, and beams and columns are defined according to the section size. The three-dimensional model (structure stereogram) is shown in Figure 3, and the load distribution on the structure is shown in Table 2 [46]. After adding the loads, plastic hinges are arranged on the beams and columns. Using the default hinge properties in the software, based on the provisions of FEMA356, p-M2-M3 coupling hinges are selected for the columns, and the positions are selected at both ends of the column as 0.1 times the length of the columns. M3 hinges are adopted for beams, and the positions are selected as 0.1 times the length of the beams from both ends [47]. Modal analysis of the established model shows that the natural vibration period of the structure is 1.119 s, and the vibration mode is x translational. According to China's Code for Seismic Design of Buildings [48], the natural vibration period of the structure is calculated as 1.0764 s, and the error is 3.8%, which is considered reasonable.
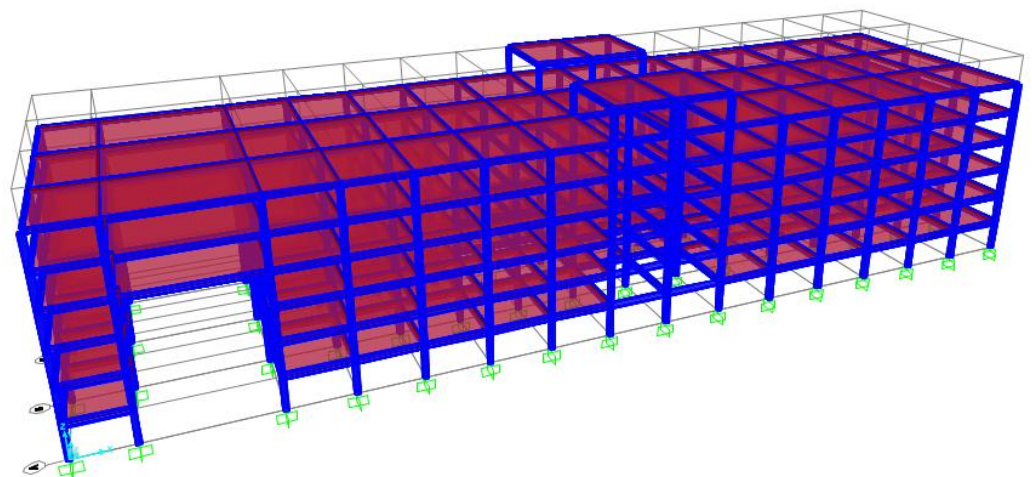


**Figure 3.** Structure stereogram.

**Table 2.** Structure load distribution.

| Function | Load Type | Load Amplitude (kN·m$^{-2}$) |
|---|---|---|
| Roof | Dead load | 7.3 |
| | Live load | 2.4 |
| Commercial store | Dead load | 4.5 |
| | Live load | 2.4 |
| Food stores | Dead load | 5.8 |
| | Live load | 1.8 |
| Parking lot | Dead load | 4.1 |
| | Live load | 2.9 |
| Stairs | Dead load | 2.2 |
| | Live load | 3.2 |

*3.2. Selection of Ground Motions and Development of Main Aftershock Sequence*

In this paper, 22 groups of far-field record set and 28 groups of near-field record set recommended by the Applied Technology Council project (ATC-63) [49] are referred to.

According to China's Standard for Seismic Resilience Assessment of Buildings [50], the principle of dual control of peak acceleration and peak velocity is adopted to make the selected ground motions meet the minimum values of PGA and PGV at the same time. In addition, the selection rules recommended by ATC-63 are also referred to. Thirteen ground motions were selected as shown in Table 3, based on the following selection rules: (1) the magnitude is greater than 6.5; (2) the PGA of each ground motion is greater than 0.2 g; (3) the PGV of each ground motion record is greater than 15 cm/s; (4) the focal mechanism of the earthquake is a thrust fault or a strike-slip layer; (5) the epicenter distance is required to be not less than 10 km; (6) the effective period of the seismic wave is greater than or equal to 4 s; (7) the predominant period of the response spectrum recorded by the ground motion is close to the characteristic period of the site. The acceleration response spectrum of ground motions is shown in Figure 4.

**Table 3.** Ground motion records.

| Number | Record Name (Event) | Earthquake Year | Magnitude | PGA (g) | PGV (cm/s) |
|---|---|---|---|---|---|
| 1 | San Fernando, U.S. | 1971 | 6.61 | 0.21 | 18.87 |
| 2 | Duzce, Turkey | 1900 | 7.14 | 0.35 | 59.99 |
| 3 | Imperial Valley, U.S.-06 | 1979 | 6.53 | 0.35 | 33.00 |
| 4 | Friuli, Italy-01 | 1976 | 6.5 | 0.35 | 22.04 |
| 5 | Irpinia, Italy-01 | 1980 | 6.9 | 0.36 | 51.84 |
| 6 | Loma Prieta, U.S. | 1989 | 6.93 | 0.56 | 35.68 |
| 7 | Kocaeli, Turkey | 1999 | 7.51 | 0.22 | 29.78 |
| 8 | Loma Prieta, U.S. | 1989 | 6.93 | 0.64 | 55.15 |
| 9 | Kobe, Japan | 1995 | 6.9 | 0.51 | 37.29 |
| 10 | Kocaeli, Turkey | 1999 | 7.51 | 0.22 | 17.69 |
| 11 | Gazli, USSR | 1976 | 6.8 | 0.72 | 71.56 |
| 12 | Imperial Valley, U.S.-06 | 1979 | 6.53 | 0.41 | 64.85 |
| 13 | Loma Prieta, U.S. | 1989 | 6.93 | 0.32 | 42.61 |

Due to the lack of a real main aftershock sequence, this paper adopts the method of artificially constructing the main aftershock sequence. The main aftershock sequence is constructed based on the repeated method, that is, the main shock is recorded directly and amplitude modulation is required to make the main shock and aftershock have similar seismic characteristics. At the same time, to ensure enough time to restore the stable state of the building structure after experiencing the main shock, the time interval of 60 s was set between the main shock and the aftershock. It is worth noting that the main aftershock sequence constructed in this paper is reconsidered as a new seismic record.
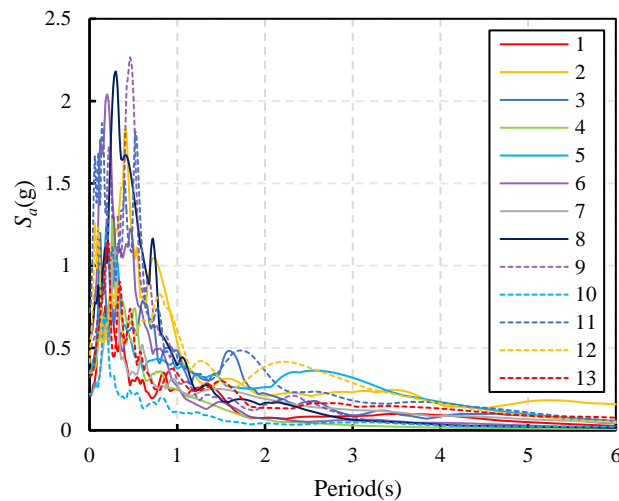
**Figure 4.** Acceleration response spectrum of ground motion.

### 3.3. Incremental Dynamic Analysis

#### 3.3.1. Using Maximum Inter-Story Drift Ratio as DM

In this paper, the damping ratio is 0.05, and the elastic response spectrum value corresponding to the first characteristic period is selected as IM. The maximum inter-story drift ratio and residual inter-story drift ratio are selected as DMs. IDA curves obtained by the Bessel interpolation formula under the action of main shock alone and main aftershock are shown in Figures 5 and 6, respectively.

The IDA curve of the main earthquake and the main aftershock were compared, and the curve of the structure considering the aftershock was more discrete and had greater randomness when $S_a(T_1,5\%)$ was larger. This shows that the steel frame gradually loses its ability to resist reciprocating load under the aftershock action; thus, the structure's response gradually shows variability. To further reduce dispersion, IDA cluster data were collected and quantile value curves of 16%, 50%, and 84% were drawn, as well as the logarithmic standard deviation of ground motion intensity corresponding to the steel frame structure under different responses, as shown in Figures 7 and 8, respectively.
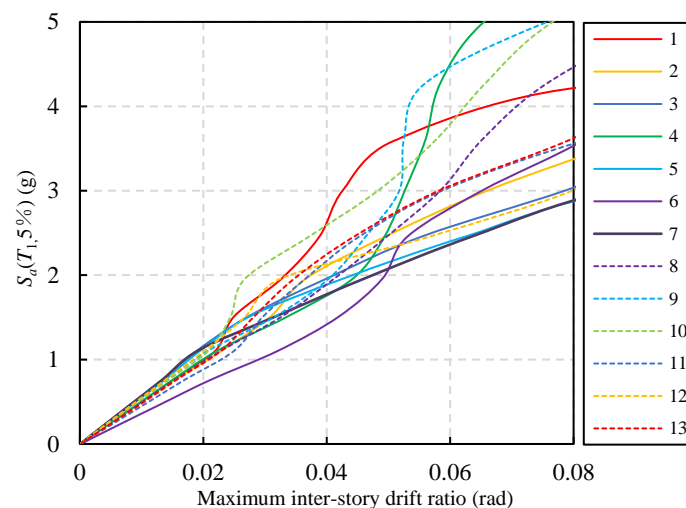


**Figure 5.** IDA curve of the maximum inter-story drift ratio under the main shock.
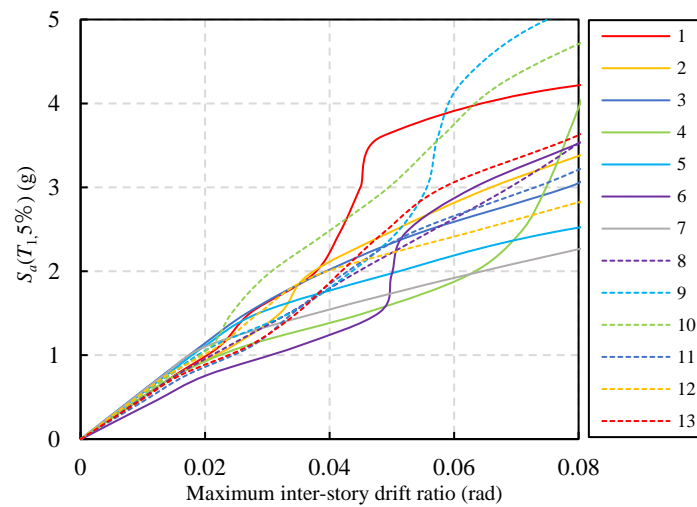
**Figure 6.** IDA curve of the maximum inter-story drift ratio under the main aftershock.
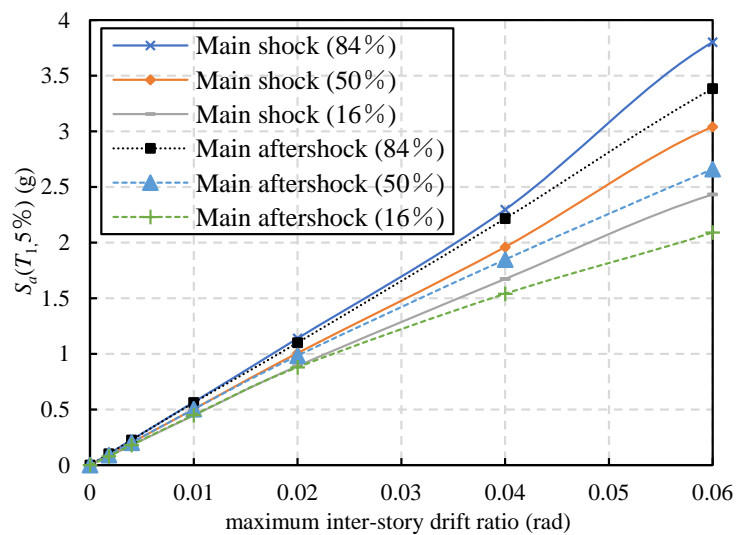


**Figure 7.** Quantile curves of the maximum inter-story drift ratio under the main shock and the main aftershock.
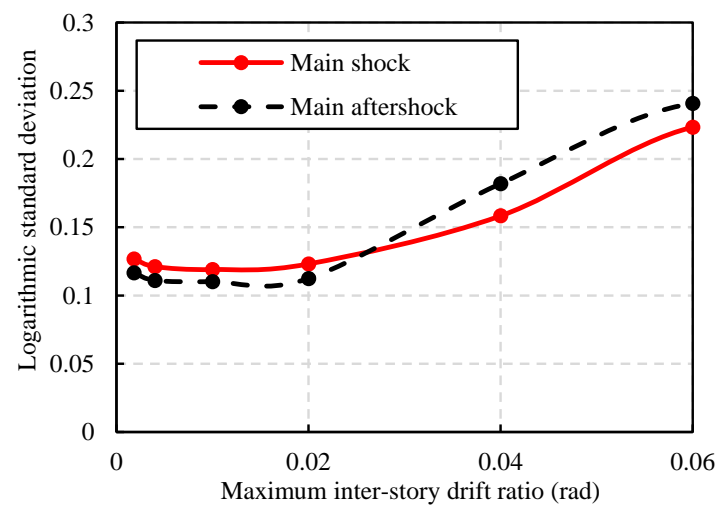


**Figure 8.** Logarithmic standard deviation of earthquake intensity under the main shock and the main aftershock.

As can be seen from Figure 7, when $S_a(T_1,5\%)$ is less than 0.5 g, the quantile value curves almost coincide, and the aftershock has no noticeable effect on the structure. However, as $S_a(T_1,5\%)$ increases, the structural response also increases, and the structures experiencing aftershocks have a greater response. This indicates that when $S_a(T_1,5\%)$ is large, the structures that have experienced the main shock are damaged to a certain extent, which makes the effect of aftershock clear and cannot be ignored.

As can be seen from Figure 8, the logarithmic standard deviation shows first a trend of flattening and then increasing, and the function of the main shock with the standard deviation in the early stage is greater than that of the main aftershock. This is because when the earthquake intensity is small, the structure is not in the inelastic phase, and the response of the structure is mainly composed of ground motion peak acceleration control. When the IDA was completed, the main after sequence is regarded as a seismic record, and $S_a(T_1,5\%)$ value will be increased, which also determined that regarding the PGA input, the structure in the elastic phase is small compared with the single earthquake coefficient. Therefore, the shaking of the structure during the main aftershock is not as obvious as the main shock.

According to China's Code for Seismic Design of Buildings [48], the displacement ratio limit of the elastic layer is 1/250, and that of the elastoplastic layer is 1/50. Combined with existing seismic collapse analysis results [51] and relevant provisions in FEMA356 (Prestandard and Commentary for the Seismic Rehabilitation of Buildings) [52], four performance levels are defined: "Normal Operation (NO)", "Immediate Occupancy (IO)", "Life Safety (LS)", and "Collapse Prevention (CP)". The corresponding structural performance index limits for each performance level are shown in Table 4 [51]. According to the quantile value curve, the Bessel interpolation formula was used to solve, and the corresponding capacity values of different performance levels of the structure were output, as detailed in Table 5.

**Table 4.** The maximum inter-story drift ratio corresponding to different performance levels.

| Structural Performance Level | Target Inter-Story Drift Index (rad) |
| --- | --- |
| Normal Operation (NO) | 1/250 |
| Immediate Occupancy (IO) | 1/100 |
| Life Safety (LS) | 1/50 |
| Collapse Prevention (CP) | 1/25 |

**Table 5.** Capability values corresponding to different performance levels.

| Quantile Values | | NO $S_a(T_1,5\%)$ (g) | IO $S_a(T_1,5\%)$ (g) | LS $S_a(T_1,5\%)$ (g) | CP $S_a(T_1,5\%)$ (g) |
| --- | --- | --- | --- | --- | --- |
| Main Shock | 16% | 0.0787 | 0.1780 | 0.4466 | 0.8902 |
| | 50% | 0.0893 | 0.2010 | 0.5031 | 1.0069 |
| | 84% | 0.1013 | 0.2269 | 0.5667 | 1.1388 |
| Main after Shock | 16% | 0.0797 | 0.1799 | 0.4501 | 0.8789 |
| | 50% | 0.0896 | 0.2010 | 0.5026 | 0.9835 |
| | 84% | 0.1007 | 0.2246 | 0.5611 | 1.1005 |

Take the 50% quantile value as an example. The $S_a(T_1,5\%)$ value of the main aftershock increases by 0.33% compared with that of the main shock in the NO stage, increases by 0.11% in the IO stage, decreases by 2.38% in the LS stage, and decreases by 8.01% in the CP stage. It is clear that as the structural response is continuously increasing, aftershocks are also playing an increasingly important role.

For further analysis, the exceedance probability difference of reaching four different performance levels under the action of the main aftershock is analyzed, as shown in Figure 9. The expression of the transcendence probability is as follows:

$$P_f = \varphi \left\{ \frac{ln\left[ a \cdot (S_s)^b / \hat{C} \right]}{\sqrt{(\beta_c^2 + \beta_d^2)}} \right\} \tag{7}$$

where $a$ and $b$ can be obtained from the seismic demand model, $\hat{C}$ is the stage point exceeding the collapse performance of the structure, $\beta_c$ is the logarithmic standard deviation of the structural seismic capacity, $\beta_d$ is the logarithmic standard deviation of the seismic demand, and $\sqrt{(\beta_c^2 + \beta_d^2)}$ equals 0.4.
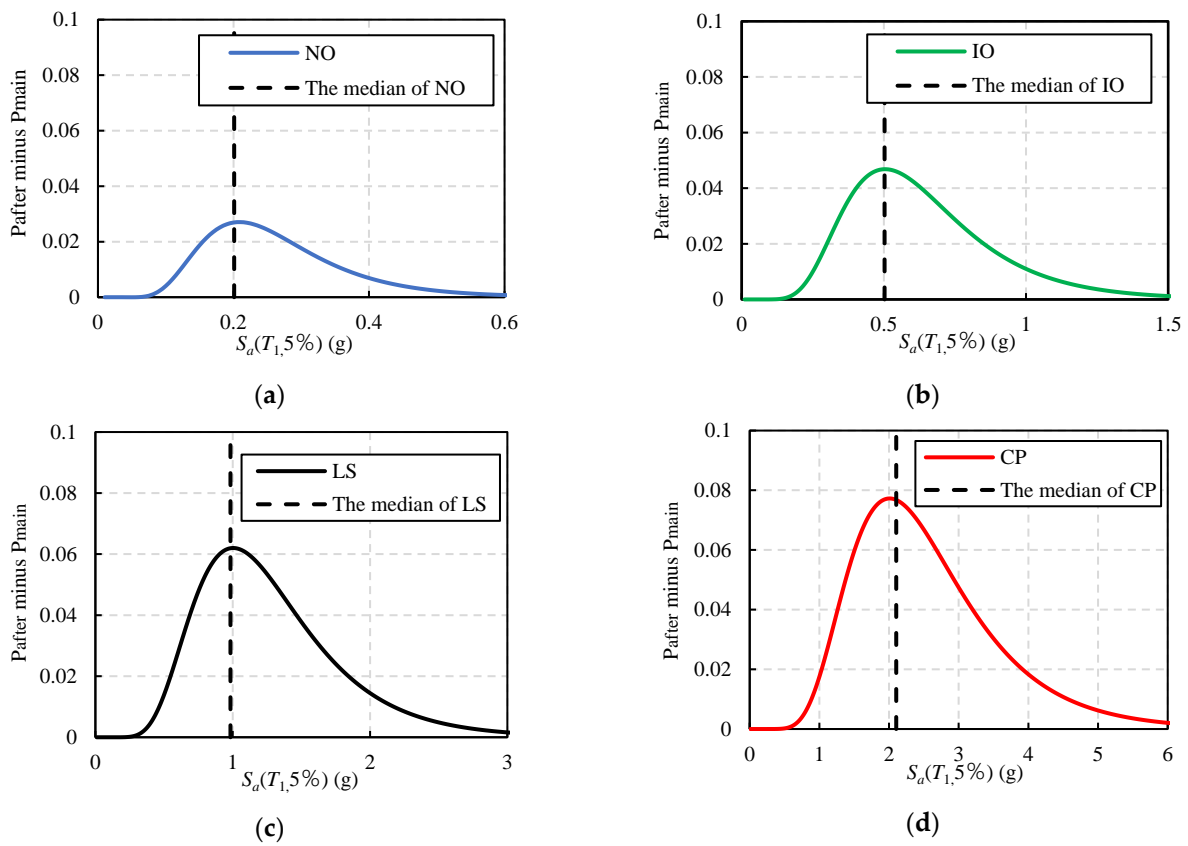


**Figure 9.** Exceedance probability difference of the main aftershock at different performance levels: (**a**) probability differentials of NO stage; (**b**) probability differentials of IO stage; (**c**) probability differentials of LS stage; and (**d**) probability differentials of CP stage.

As can be seen in Figure 9, the peak value of the probability difference increases continuously from NO, IO, LS, to CP stage. The larger the peak value is, the larger the difference between the response of the structure that experienced the main shock and main aftershock is. Simultaneously, the peak value of probability difference in different stages gradually moved to the right, and the relative position of median and peak value also changed. Overall, the median also moved to the right relative to the peak. In the NO stage, most $S_a(T_1,5\%)$ values of the ground motion intensity index are too small to cause damage to the steel frame; thus, the maximum value of the probability difference between the main aftershock appears after the median value. As the limit stage of performance level increases, the corresponding ground motion intensity also increases; therefore, the cumulative damage of the steel frame increases, leading to a higher probability of structural failure. In addition, the distance between the abscissa of the highest point and the dotted

line is getting more closer, which indicates that in a higher limit stage, the damage of the structure has reached a certain degree, and the ground motion intensity index does not need to further increase to cause the damage in the structure. Therefore, it can be inferred that if the structural stiffness is reduced to make the structure suffer more serious damage under the same ground motion intensity, the median may also appear after the peak value.

### 3.3.2. Using Residual Inter-Story Drift Ratio as DM

The residual inter-story drift ratio was used as the DM to carry out the IDA under the action of the main earthquake and main aftershock, respectively, and draw the IDA curve as shown in Figures 10 and 11.
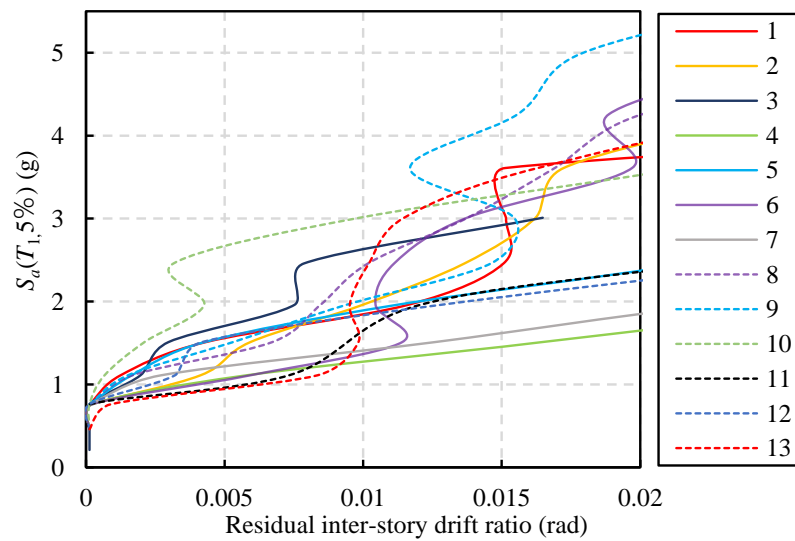


**Figure 10.** IDA curve of residual inter-story drift ratio under the main shock.
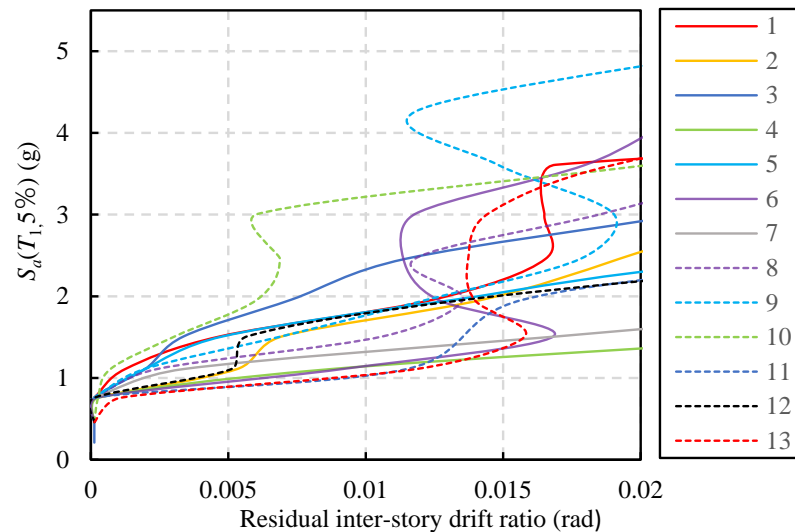


**Figure 11.** IDA curve of residual inter-story drift ratio under the main aftershock.

Compared with the maximum inter-story drift ratio, the residual inter-story drift ratio curve is more discrete and has more hardening stages because the residual inter-story drift ratio is affected by the seismic polarity and the recovery property of the structure itself. To make the data clearer, a quantile value curve is drawn, as shown in Figure 12.
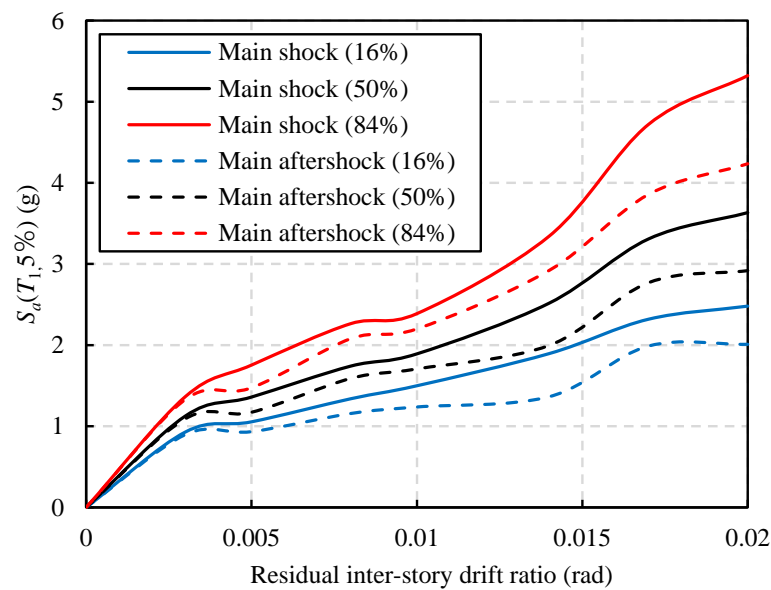
**Figure 12.** IDA quantile curve of residual inter-story drift ratio under the main aftershock.

As can be seen from Figure 12, the curve under the action of the main aftershock is always below that under the action of the main shock. Considering the 50% fractional value curve as an example, when the residual inter-story drift ratio under the main shock reaches 0.02, the median intensity of the corresponding ground motion is 3.66 g. When the residual inter-story drift ratio under the main aftershock reaches 0.02, the median intensity of ground motion is 2.92 g. Considering the effect of the aftershocks, the earthquake intensity to let the structure reach the same residual inter-story drift ratio is reduced by 20.22%.

To further analyze the influence of residual inter-story drift ratio and maximum inter-story drift ratio on the IDA results, the structural response value corresponding to the 50% fractional value is obtained according to the capacity value in Table 5 and the data value in Figure 12, and the ratio of the two inter-story drift ratios is calculated. The results are shown in Tables 6 and 7.

**Table 6.** Inter-story drift ratio and ratios of two layers under the action of the main shock.

| Stage | Maximum Inter-Story Drift Ratio (rad) | $S_a(T_1,5\%)$ Median (g) | Residual Inter-Story Drift Ratio (rad) | Ratio (Maximum/Residual) |
|---|---|---|---|---|
| NO | 0.004 | 0.2010 | 0.00052 | 7.712 |
| IO | 0.01 | 0.5031 | 0.00127 | 7.863 |
| LS | 0.02 | 1.0069 | 0.00260 | 7.673 |
| CP | 0.04 | 2.1035 | 0.01113 | 3.594 |

**Table 7.** Inter-story drift ratio and ratios of two layers under the action of the main aftershock.

| Stage | Maximum Inter-Story Drift Ratio (rad) | $S_a(T_1,5\%)$ Median (g) | Residual Inter-Story Drift Ratio (rad) | Ratio (Maximum/Residual) |
|---|---|---|---|---|
| NO | 0.004 | 0.2010 | 0.00053 | 7.547 |
| IO | 0.01 | 0.5026 | 0.00129 | 7.748 |
| LS | 0.02 | 0.9835 | 0.00260 | 7.631 |
| CP | 0.04 | 1.9475 | 0.01337 | 2.992 |

According to the results in Tables 6 and 7, except when the structure enters the CP state, the ratio of the maximum inter-story drift ratio to the residual inter-story drift ratio is between 7.5 and 7.9, and the ratio under the action of the main aftershock is smaller than that under the action of the main earthquake. Therefore, it can be inferred that the variation range of the residual inter-story drift ratio is greater than the maximum inter-story drift ratio after the aftershock, and the residual inter-story drift ratio is more sensitive than the

maximum inter-story drift ratio during the incremental dynamic analysis or vulnerability analysis of the structure under the main aftershock.

### 3.3.3. Using Two Inter-Story Drift Ratios as DMs

To further explore the relationship between the two inter-story drift ratios and earthquake intensity, and to analyze the correlation between the two indices, this section uses the above two types of inter-story drift ratios as the independent variables and the $S_a(T_1,5\%)$ as the dependent variable, according to the data distribution under different earthquake intensity, to explore the influence of double-index model for vulnerability analysis.

Considering the randomness of the inter-story drift ratio of the steel frame structure under the seismic action, it is assumed that the distribution of the maximum inter-story drift ratio and the residual inter-story drift ratio is a 2-D lognormal distribution under the condition that the intensity of ground motion is determined.

Therefore, the probability density function can be expressed as follows:

$$f(x,y) = \left(2\pi\sigma_1\sigma_2\sqrt{1-\rho^2}\right)^{-1} \exp\left[-\frac{1}{2(1-\rho^2)}\left(\frac{(x-\mu_1)^2}{\sigma_1^2} - \frac{2\rho(x-\mu_1)(y-\mu_2)}{\sigma_1\sigma_2} + \frac{(y-\mu_2)^2}{\sigma_2^2}\right)\right] \quad (8)$$

where $\sigma_1$ and $\sigma_2$ represent the standard deviations of data $x$ and $y$, respectively; $\mu_1$ and $\mu_2$ represent the mean values of data $x$ and $y$, respectively; and $\rho$ stands for the correlation coefficient with a value range of [−1, 1]. The calculation method is as follows:

$$\rho = \frac{Cov(x,y)}{\sigma_1\sigma_2} \quad (9)$$

where $Cov(x,y)$ represents the covariance of data $x$ and $y$.

The data when $S_a(T_1,5\%) = 2.0$ g were analyzed as an example, and the joint probability density diagram was obtained, as shown in Figures 13 and 14.



(a)

(b)
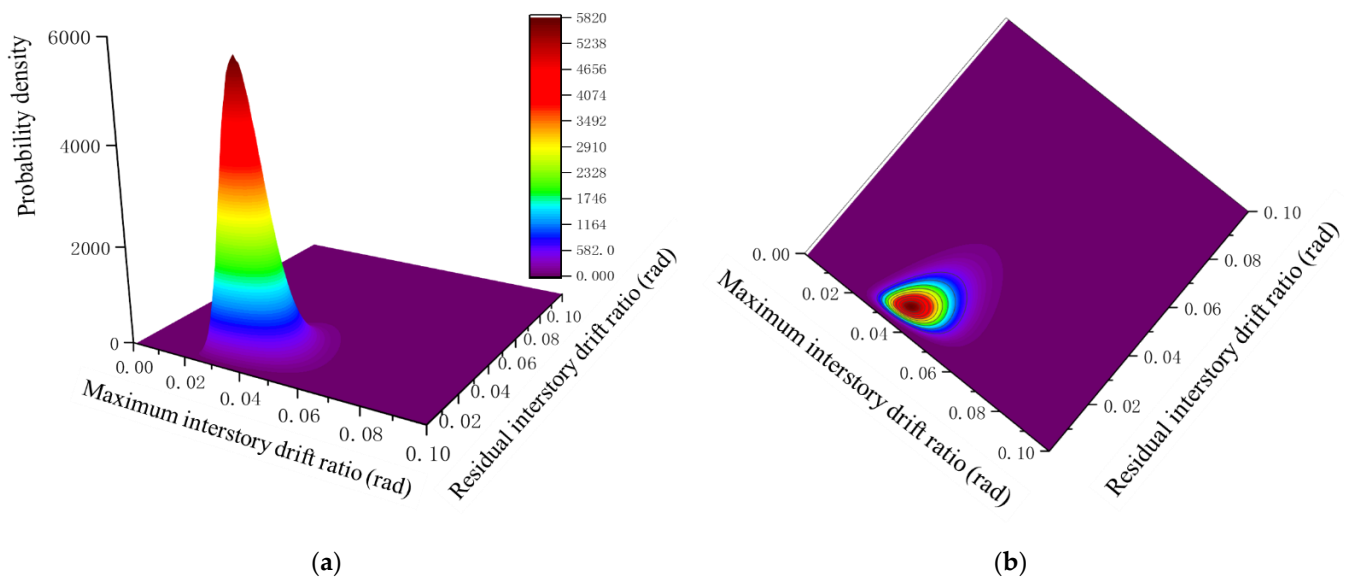
**Figure 13.** Joint probability density function of structural response under the main shock when $S_a(T_1,5\%) = 2.0$ g: (**a**) joint probability density function diagram; and (**b**) top view of the joint probability density function.

(**a**)                                        (**b**)
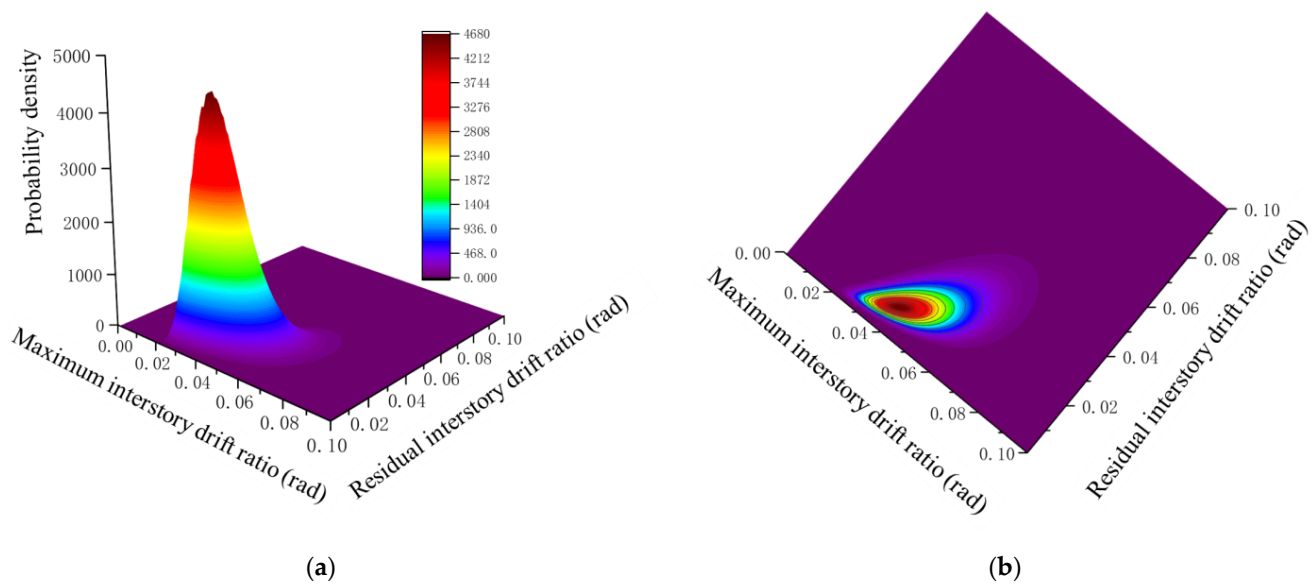
**Figure 14.** Joint probability density function of structural response under the main aftershock when $S_a(T_1,5\%) = 2.0$ g: (**a**) joint probability density function diagram; and (**b**) top view of the joint probability density function.

It can be seen from Figures 13 and 14 that the peak value of the joint probability distribution function under the action of the main shock is significantly greater than that under the action of the main aftershock, indicating that the aftershock increases the discrete degree of multiple structural responses. It is found that the maximum inter-story drift ratio did not significantly change, but the residual inter-story drift ratio increased slightly under the aftershock. Comparing the top view, it is found that under the action of the main shock, the probability density function is relatively uniform. However, under the action of the main aftershock, the graphics significantly elongated, and the variation range of the residual inter-story drift ratio is more significant. It indicates that the structure's control over the maximum inter-story drift ratio and residual inter-story drift ratio will be weakened, and its control over the residual inter-story drift ratio will be weaker under the action of the main aftershocks.

The results show that under the action of the main shock and the main aftershock, there is an obvious positive linear correlation between the maximum inter-story drift ratio and the residual inter-story drift ratio. In other words, the residual inter-story drift ratio is largely affected by the maximum inter-story drift ratio during an earthquake. Therefore, using the two-dimensional lognormal distribution to analyze the structural vulnerability can improve the calculation accuracy, while using the one-dimensional lognormal distribution of a single index to analyze separately will increase the first type error probability. In addition, in the normal joint distribution, the transcendence probability calculation results for the maximum inter-story drift ratio and the residual inter-story drift ratio will be accurate, rather than the calculation of probability multiplication using the two- and one-dimensional normal distributions alone, which improves the accuracy of the calculation.

The maximum inter-story drift ratio of 0.02 and the residual inter-story drift ratio of 0.01 were selected as the limits in this study. One-dimensional and two-dimensional lognormal distributions were used to calculate the exceedance probability of the structure under the action of the main earthquake and the main aftershock, respectively. The calculation results are shown in Tables 8 and 9. The relative error of exceedance probability is shown in Figure 15.

**Table 8.** Exceedance probability under the main shock.

| $S_a$ (T$_1$,5%) | One-Dimensional Lognormal Distribution | | | Two-Dimensional Lognormal Distribution |
|---|---|---|---|---|
| | Maximum Inter-Story Drift Ratio Exceeds the Limit | Residual Inter-Story Drift Ratio Exceeds the Limit | Transfinite (Mutual Independence) | Transfinite (Correlative) |
| 1.0 | 0.5223 | $2.519 \times 10^{-86}$ | 0.5223 | 0.7593 |
| 1.2 | 0.6909 | $1.266 \times 10^{-53}$ | 0.6909 | 0.9684 |
| 1.4 | 0.8086 | $3.538 \times 10^{-38}$ | 0.8086 | 0.9957 |
| 1.6 | 0.8843 | $5.932 \times 10^{-3}$ | 0.8850 | 0.9999 |
| 1.8 | 0.9309 | $3.689 \times 10^{-2}$ | 0.9335 | 1.0000 |
| 2.0 | 0.9589 | $1.278 \times 10^{-1}$ | 0.9642 | 1.0000 |

**Table 9.** Exceedance probability under the main aftershock.

| $S_a$ (T$_1$,5%) | One-Dimensional Lognormal Distribution | | | Two-Dimensional Lognormal Distribution |
|---|---|---|---|---|
| | Maximum Inter-Story Drift Ratio Exceeds the Limit | Residual Inter-Story Drift Ratio Exceeds the Limit | Transfinite (Mutual Independence) | Transfinite (Correlative) |
| 1.0 | 0.5843 | $2.263 \times 10^{-86}$ | 0.5842 | 0.8055 |
| 1.2 | 0.7471 | $8.496 \times 10^{-53}$ | 0.7471 | 0.9759 |
| 1.4 | 0.8527 | $4.584 \times 10^{-37}$ | 0.8527 | 0.9972 |
| 1.6 | 0.9161 | $2.251 \times 10^{-2}$ | 0.9180 | 0.9999 |
| 1.8 | 0.9527 | $1.049 \times 10^{-1}$ | 0.9577 | 1.0000 |
| 2.0 | 0.9734 | $2.798 \times 10^{-1}$ | 0.9808 | 1.0000 |
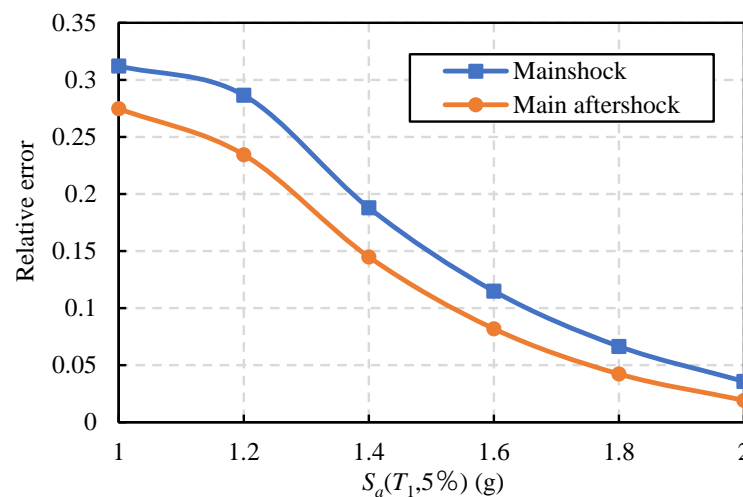


**Figure 15.** Exceedance Probability Relative Errors from One- and Two-dimensional Lognormal Distributions.

It can be seen from the results in Tables 8 and 9 that the exceedance probability calculated by the one-dimensional lognormal distribution is quite different from that calculated by the two-dimensional lognormal distribution. The two-dimensional distribution probability constant is greater than the one-dimensional distribution. It indicates that the structure has a higher probability of exceeding the limit after considering the correlation of the two indices. As can be seen from Figure 15, calculation results when the structure is subjected to smaller underground motion intensity have a greater error, when $S_a$(T$_1$,5%) = 1.0 g, the relative error under the main shock is more than 30%, and the relative error under the main aftershock is more than 25%. With increasing seismic intensity, the relative error gradually

decreases, and the distance between the two curves, which represents the relative error between the main shock and the main aftershock, is also falling. At the same time, the relative error calculated under the main shock is greater than that under the main aftershock.

To explore the influence of different DMs on the results of structural vulnerability analysis under the condition of the two-dimensional normal distribution, the exceedance probability is divided into three zones, as shown in Table 10. The exceedance probability distribution of each zone is obtained, as shown in Figures 16 and 17. As can be seen from Figures 16 and 17, the exceedance probability is mainly composed of zone II and zone III. With the gradual increase of ground motion intensity, the proportion of zone III increases gradually, but zone II decreases gradually, and the proportion of zone III is larger under the action of the main aftershocks. The results show that when the ground motion intensity increases, the part of maximum inter-story drift ratio and residual inter-story drift ratio simultaneously exceeding the limit will have a greater impact on vulnerability analysis, and the aftershocks will increase this effect. Therefore, under the action of the greater intensity of the earthquake, vulnerability analysis based on the IDA should focus on the maximum inter-story drift ratio and residual inter-story drift ratio, simultaneously exceeding the limit.

**Table 10.** Partition of exceedance probability.

| Zone | Represent |
| --- | --- |
| Zone I | Only the residual inter-story drift ratio limit was reached |
| Zone II | Only the maximum inter-story drift ratio limit was reached |
| Zone III | Both the residual inter-story drift ratio and the maximum inter-story drift ratio reached the limits at the same time |
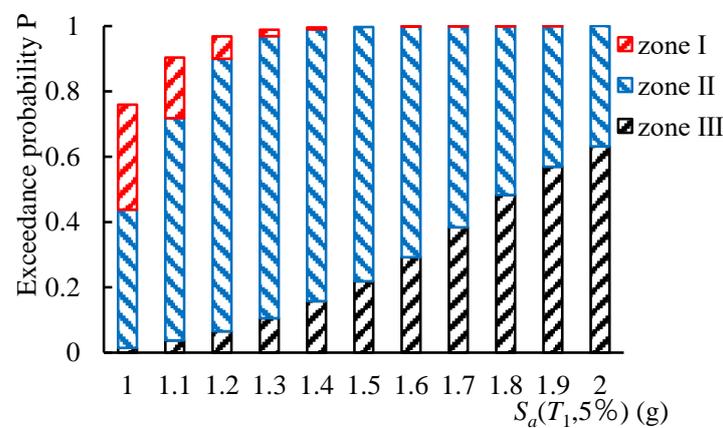


**Figure 16.** Exceedance probability distribution under the action of the main shock.
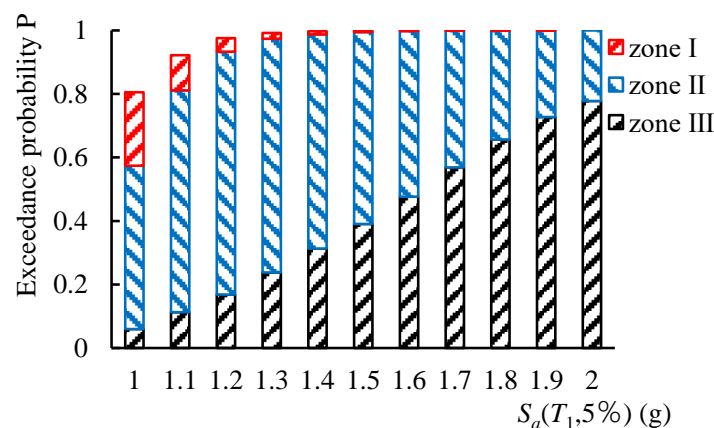


**Figure 17.** Exceedance probability distribution under the action of the main aftershock.

## 4. Conclusions

A method of IDA analysis based on two indices is proposed in this paper. The maximum and the residual inter-story drift ratios were selected as two DMs to conduct the IDA based on the correlation of two indices for a steel frame. The impact of aftershocks on the seismic performance of buildings was evaluated by comparing the structural response under the action of both the main earthquake and the main aftershock, and the impact of the correlation of the two indices on the structural vulnerability was also evaluated. The main conclusions were as follows:

1.  When selecting the two indices for IDA and vulnerability analysis, the correlation between the two indices can be more accurately considered by adopting the two-dimensional lognormal distribution, compared with the one-dimensional normal distribution, and more convincing exceedance probability can be obtained, which solves the problem that the exceedance probability is not unique when the single-index IDA is used. Moreover, the computational efficiency of double-index IDA is not affected.
2.  The larger the ground motion intensity is, the greater the proportion of the probability that the maximum and residual inter-story drift ratio exceeds the limit simultaneous to the total overrun probability of the structure; that is, the simultaneous over-limit situation will increase the influence on the structural vulnerability analysis, and the effect of aftershocks will increase this influence.
3.  During the vulnerability analysis under the action of main aftershocks, in addition to considering the maximum inter-story drift ratio, more attention should be paid to the influence of the residual inter-story drift ratio on the repairability of the structure.
4.  When experiencing the same earthquake intensity, the structural response increases noticeably considering the aftershock effect.
5.  The IDA curve drawn by the cubic Bezier interpolation function is smooth without mutation, and in the subsequent vulnerability analysis, the data can be obtained quickly, which makes data processing easier.
6.  The purpose of this method is essentially to consider the different seismic performance of a structure in a more diversified way in IDA. Therefore, this method is not applicable if only one index is required for analysis purposes.

**Author Contributions:** J.Q.: Conceptualization, Methodology, Validation, Writing—Review and Editing, Supervision; C.P.: Software, Data Curation, Writing—Original Draft, Review and Editing. All authors have read and agreed to the published version of the manuscript.

**Institutional Review Board Statement:** Not available.

**Informed Consent Statement:** Not available.

**Data Availability Statement:** Not available.

**Conflicts of Interest:** The authors declare no conflict of interest.

## References

1.  Ruiz, G.J. Mainshock-Aftershock Ground Motion Features and Their Influence in Building's Seismic Response. *J. Earthq. Eng.* **2012**, *16*, 719–773. [CrossRef]
2.  Zhong, Q.; Shi, B.P. Aftershock duration of the 1976 Ms7.8 Tangshan earthquake and implication for seismic hazard estimation. *Acta Seismol. Sin.* **2012**, *34*, 494–508, 580.
3.  Egill, H.; Lucile, M.J.; Kate, H. The 1994 Northridge earthquake sequence in California: Seismological and tectonic aspects. *J. Geophys. Res.* **1995**, *100*, 12335–12355. [CrossRef]

4.   Li, H.N.; Xiao, S.Y.; Huo, L.S. Damage investigation and analysis of engineering structures in the Wenchuan earthquake. *J. Build. Struc.* **2008**, 10–19. [CrossRef]

5.   Sammonds, P.; Pomonos, A.; Fraser, S. Ground motion characteristics and shaking damage of the 11th March 2011 M_w9.0 Great East Japan earthquake. *Bull. Earthq. Eng.* **2013**, *11*, 141–170. [CrossRef]

6.   Zhang, C.J.; Hou, Y.Y.; Hu, B.; Xu, H.H.; Wang, D.B. Analysis on the seismic actives and hazards of M7.1 earthquake, 2010 and M6.3 earthquake, 2011 in New Zealand. *Prog. Earthq. Sci.* **2011**, *4*, 9, 44–51.

7.   Comerio, M.; Elwood, K.; Berkowitz, R. *The M6.3 Christchurch, New Zealand, Earthquake of 22 February 2011*; Earthquake Engineering Research Institute (EERI): Oakland, CA, USA, 2011.

8.   Chen, J.; Zhai, G.F.; Li, S.S. Thoughts, measures and progress of reconstruction after the "3.11" Great East Japan Earthquake. *Urban Plan. Int.* **2012**, *27*, 123–127.

9.   Roy, A.; Chakraborty, S. Reliability analysis of structures by a three-stage sequential sampling based adaptive support vector regression model. *Reliab. Eng. Syst. Safe.* **2022**, *219*, 108260. [CrossRef]

10.  Akkar, S.; Cheng, Y. Application of a Monte-Carlo simulation approach for the probabilistic assessment of seismic hazard for geographically distributed portfolio. *Earthq. Eng. Struct. D.* **2016**, *45*, 525–541. [CrossRef]

11.  Gaxiola-Camacho, J.R.; Azizsoltani, H.; Villegas-Mercado, F.J.; Haldar, A. A novel reliability technique for implementation of Performance-Based Seismic Design of structures. *Eng. Struct.* **2017**, *142*, 137–147. [CrossRef]

12.  Zhang, Y.H.; Li, Q.S.; Lin, J.H.; Williamsc, F.W. Random vibration analysis of long-span structures subjected to spatially varying ground motions. *Soil Dyn. Earthq. Eng.* **2009**, *29*, 620–629. [CrossRef]

13.  Bertero, V.V. Strength and Deformation Capacities of Buildings under Extreme Environments. *Struct. Eng. Mech.* **1977**, *53*, 29–79.

14.  Vamvatsikos, D.; Cornell, A. Incremental dynamic analysis. *Earthq. Eng. Struct. Dyn.* **2002**, *31*, 491–514. [CrossRef]

15.  Mofid, S.; Zarfam, P.; Raeisifard, B. On the modal incremental dynamic analysis. *Struct. Des. Tall. Spec.* **2005**, *14*, 315–329. [CrossRef]

16.  Han, S.W.; Chopra, A.K. Approximate incremental dynamic analysis using the modal pushover analysis procedure. *Earthq. Eng. Struct. Dyn.* **2006**, *35*, 1853–1873. [CrossRef]

17.  Li, N.; Zhai, C.H.; Xie, L.L. Simplified increment dynamic analysis method for uniaxial plan asymmentric structures. *Eng. Mech.* **2011**, *28*, 8–12. [CrossRef]

18.  Wang, M.F.; Wang, Z.H.; Liu, F.F. Improved method for incremental dynamic analysis and its application. *Earthq. Eng. Eng. Dyn.* **2012**, *32*, 30–35. [CrossRef]

19.  Hao, R.X.; Yang, Z.X.; Li, G.; Yu, D.H.; Jia, S. Incremental dynamic analysis method based on force analogy method. *J. Vib. Shock.* **2019**, *38*, 175–183, 190. [CrossRef]

20.  Zhou, Y.; Lu, X.L.; Bo, Y. Application of Incremental Dynamic Analysis to Seismic Evaluation of Hybrid Structure. *J. Tongji. Univ.* **2010**, *38*, 183–187, 193.

21.  Wu, Q.Y.; Zhu, H.P.; Fan, J. Seismic performance evaluation of steel moment resisting frames using incremental dynamic analysis. *J. Huazhong. Univ. Sci. Tech.* **2012**, *40*, 35–39. [CrossRef]

22.  Charney, F.A. Applications in Incremental Dynamic Analysis. In Proceedings of the ASCE Structures Congress 2005, New York, NY, USA, 20–24 April 2005. [CrossRef]

23.  Meng, C.; Tang, L. Seismic fragility analysis of pile-supported wharf in nearshore liquefiable ground. *Chin. J. Geotech. Eng.* **2021**, *43*, 2274–2282.

24.  Wan, H.P.; Wei, Z.C.; Su, L.; Ren, W.X. Seismic risk analysis of bridge structure considering pile diameter effect. *J. Vib. Shock.* **2021**, *40*, 224–231. [CrossRef]

25.  Zhong, Z.L.; Yan, Z.H.; Shi, Y.B.; Zhao, M.; Du, X. Seismic Performance Evaluation of Station Structures Based on IDA Method. *J. Beijing Univ. Tech.* **2021**, *47*, 680–690.

26.  Ren, H.; Tian, Q.H.; Zhang, W.C.; Zhou, C.F.; Shao, D. Seismic fragility analysis of reinforced concrete frame structures based on IDA method. *Build. Struc.* **2019**, *49*, 350–355. [CrossRef]

27.  Liel, A.B.; Haselton, C.B.; Deierlein, G.G. Seismic Collapse Safety of Reinforced Concrete Buildings. II: Comparative Assessment of Nonductile and Ductile Moment Frames. *J. Struct. Eng.* **2011**, *137*, 492–502. [CrossRef]

28.  ASCE. *Minimum Design Loads for Buildings and Other Structures*; ASCE/SEI 7-10; ASCE: New York, NY, USA, 2013. [CrossRef]

29.  Jalayer, F.; Franchin, P.; Pinto, P.E. A scalar damage measure for seismic reliability analysis of RC frames. *Earthquake Engng Struct. Dyn.* **2007**, *36*, 2059–2079. [CrossRef]

30.  Nazari, N.; Lindt, J.W.; Li, Y. Effect of Mainshock-Aftershock Sequences on Wood frame Building Damage Fragilities. *J. Perform. Constr. Fac.* **2013**, 04014036. [CrossRef]

31.  Jeon, J.S.; DesRoches, R.; Lowes, L.N.; Brilakis, I. Framework of aftershock fragility assessment–case studies: Older California reinforced concrete building frames. *Earthq. Eng. Struct. Dyn.* **2015**, *44*, 2617–2636. [CrossRef]

32.  Mohammad, R.S.; Mohammad, M.K.; Katsuichiro, G. Influence of advanced structural modeling technique, mainshock-aftershock sequences, and ground-motion types on seismic fragility of low-rise RC structures. *Soil. Dyn. Earth. Eng.* **2019**, *117*, 263–279. [CrossRef]

33.  Sarno, L.D.; Wu, J.R. Fragility assessment of existing low-rise steel moment-resisting frames with masonry infills under mainshock-aftershock earthquake sequences. *Bull. Earthq. Eng.* **2021**, *19*, 2483–2504. [CrossRef]

34.  Marina, P.; Valentina, G.; Francesco, C.; Stefano, L. Aftershock fragility assessment of Italian cast–in–place RC industrial structures with precast vaults. *J. Build. Eng.* **2020**, *29*, 101206.1–101206.18. [CrossRef]

35.  Yang, Y.F.; Xiao, C.; Tan, X. Fragility Analysis of Step-terrace Frame Structures on the Slope under Mainshock and Aftershocks. *Chin. Earthq. Eng. J.* **2020**, *42*, 290–298.

36.  Zhao, C.F.; Zhou, L.; Yu, A.; Peng, T. Fragility analysis of nuclear island structure under mainshock-aftershock sequences. *Earthq. Eng. Eng. Vibrat.* **2021**, *41*, 113–121. [CrossRef]

37.  Baikuntha, S.; Osman, E. Aftershock fragility assessment of steel moment frames with self-centering dampers. *Eng. Struct.* **2018**, *168*, 12–22. [CrossRef]

38.  Xu, J.F.; Chen, J.; Ding, G. Fragility analysis and life cycle cost assessment of RC frame under mainshock-aftershock seismic sequences through IDA. *Earthq. Eng. Eng. Vibrat.* **2015**, *35*, 206–212. [CrossRef]

39.  Shi, F.; Gokhan, S.; Osman, E.; Zhou, Y. Risk-based mainshock-aftershock performance assessment of SMA braced steel frames. *Eng. Struct.* **2020**, *212*, 110506.1–110506.14. [CrossRef]

40.  Baker, J.W.; Cornell, C.A. A Vector-Valued Ground Motion Intensity Measure Consisting of Spectral Acceleration and Epsilon. *Earthq. Eng. Struct. Dyn.* **2005**, *34*, 1193–1217. [CrossRef]

41.  Vamvatsikos, D.; Cornell, C.A. Developing Efficient Scalar and Vector Intensity Measures for IDA Capacity Estimation by Incorporating Elastic Spectral Shape Information. *Earthq. Eng. Struct. Dyn.* **2005**, *34*, 1573–1600. [CrossRef]

42.  Bojorquez, E.; Iervolino, I. Spectral Shape Proxies and Nonlinear Structural Response. *Soil Dyn. Earthq. Eng.* **2011**, *31*, 996–1008. [CrossRef]

43.  Kazantzi, A.K.; Vamvatsikos, D. Intensity Measure Selection for Vulnerability Studies of Building Classes. *Earthq. Eng. Struct. Dyn.* **2015**, *44*, 2677–2694. [CrossRef]

44.  Eads, L.; Miranda, E.; Lignos, D.G. Average Spectral acceleration as an intensity measure for collapse risk assessment. *Earthq. Eng. Struct. Dyn.* **2015**, *44*, 2057–2073. [CrossRef]

45.  Mohammed, G.A.; Hou, M. Optimization of Active Muscle Force–Length Models Using Least Squares Curve Fitting. *IEEE Trans. Bio-Med. Eng.* **2016**, *63*, 630–635. [CrossRef] [PubMed]

46.  Wang, L.J.; Lu, L.J.; Yu, H.Q.; Tan, J.P.; Zhao, L.; Feng, D.M.; Liu, L.J. Comparison of steel frame structural design examples under Chinese and Japanese standards. *Build. Struct.* **2019**, *49*, 1–9, 17. [CrossRef]

47.  Jin, B. *Design Calculation Example of High-Rise Steel Structure*; Architecture and Building Press: Beijing, China, 2018.

48.  Ministry of Housing and Urban-Rural Construction of the People's Republic of China. *Code for Seismic Design of Buildings*; GB 50011-2010; Architecture and Building Press: Beijing, China, 2010.

49.  Federal Emergency Management Agency. *FEMA-P695 Quantification of Building Seismic Performance Factors (ATC-63 Project Report)*; The American Society of Civil Engineers: Washington, DC, USA, 2008.

50.  Ministry of Housing and Urban-Rural Construction of the People's Republic of China. *Standard for Seismic Resilience Assessment of Buildings*; GB/T 38591-2020; Architecture and Building Press: Beijing, China, 2020.

51.  Xu, Q.; Zheng, S.S.; Han, Y.Z.; Cheng, Y.; Tian, J. Steel frame seismic vulnerability based on a global structural damage index. *J. Vib. Shock.* **2014**, *33*, 78–82, 106. [CrossRef]

52.  Federal Emergency Management Agency. *FEMA 356 Prestandard and Commentary for Seismic Rehabilitation of Buildings*; The American Society of Civil Engineers: Washington, DC, USA, 2000.